Development and Control of Electrohydraulic Soft Actuators for Soft Robotics

by

Michael da Silva

A Thesis

Submitted to the Faculty

of the

WORCESTER POLYTECHNIC INSTITUTE

In partial fulfillment of the requirements for the

Degree of Masters of Science

in

Robotics Department

by

September 2024

APPROVED:

Dr. Cagdas D. Onal, Advisor

Dr. Siavash Farzan, Adjunct Professor

Dr. Kevin Leahy, Assistant Professor

Abstract

In this work, we develop and characterize electrohydraulic soft actuators to be used as wearable haptic actuators to provide realistic kinesthetic force feedback on the fingers of a user. Electrohydraulic haptic muscles, which integrate electrostatic actuation with hydraulic force, have unlocked an alternative to pneumatic muscles for haptics. The actuator uses electrostatic forces to push dielectric liquid encapsulated inside a flexible, hermetic pouch, mimicking the contraction and relaxation of a human tendon, resulting in a true-to-life motion that can be controlled with an applied voltage. We present the modeling, design, fabrication, and testing of eletrohydraulic soft actuators. To achieve electrostatic actuation, the system requires high voltages, thereby fettering the user. Therefore, a custom, adjustable, and affordable high-voltage portable power supply is presented, making these muscles a practical solution for real-world applications in wearable robotics, soft robotics, and virtual reality. Our experimental results indicate that the proposed electrohydraulic muscles offer an adaptable and cost-effective way to create natural, responsive haptic interactions.

Acknowledgements

I want to extend my sincerest appreciations to my advisor, Dr. Cagdas Onal, for his support, guidance, and mentorship during my time at the Soft Robotics Laboratory. Additionally, I'm eternally grateful to Dr. Siavash Farzan for his kindness and for lending a ear when times were rough during my degree. I also thank Dr. Kevin Leahy for being a committee member on short notice and providing feedback. My heartfelt thanks to the members of the Soft Robotics Laboratory, especially Aditi Pawaskar and Alan Pham, whose assistance and support made me get this far. Additionally, I would like thank my dear friend Emilio for always giving his words of support, and providing a motivation boost. Lastly, I would like to thank Sharon Kelting, Jessica de Oliveria, and Pauline Joncas for their invaluable aid acquiring lab supplies throughout my thesis.

Contents

List of Figures

List of Tables

Chapter 1

Introduction

When we think of robots, we often picture machines with rigid, mechanical movements—clunky motions that are unmistakably "robotic." Traditional robots, driven by hard actuators like electric motors, hydraulic pistons, and pneumatic cylinders, are powerful and precise but lack the fluidity of natural movement. These hard actuators, typically comprising plastics and metals, have a Young's modulus on the order of 10^9 to 10^{12} Pa [1]. Their uncompliant, jerky motions work well in controlled environments like factories. However, they fall short when interacting safely with humans or nature around us, manipulating delicate objects, and adapting to complex, unpredictable surroundings.

As the gap between robots in factories and those entering our homes narrows, the mechanical rigidity inherent in traditional systems poses a significant limitation. Soft actuators offer a compelling solution to this challenge by allowing robots to bend, stretch, and mimic the smooth, organic motions observed in humans and nature. Since human muscles, tissues, and skin possess a Young's modulus ranging from 10^4 to 10^9 Pa, soft actuators are often designed with bio-inspiration in mind, using smart materials that closely mimic the mechanical properties of these biological

tissues [1] [2] [3]. These actuators, functioning as transducers, deform in response to external stimuli, enabling them to generate displacement or force [4]. These stimuli can include thermal variations, electrical inputs, fluidic pressure, magnetic fields, or even changes in pH. When triggered, soft actuators undergo significant shape changes—such as bending, stretching, or contracting—producing mechanical energy. This energy can then be harnessed to perform tasks, such as gripping and manipulating heterogeneous objects or generating locomotion.

Chapter 2

Literature Review

Dielectric elastomer actuators (DEAs) are compliant, soft, and stretchable actuators that change shape in response to a large electric field, typically on the order of kilovolts. They are the basis of most of the soft actuators currently being researched, as they closely resemble human muscles [5]. DEAs are typically composed of an elastomer (such as rubber, silicone, or acrylic) sandwiched by compliant electrodes (such as carbon grease or graphite powder). When an external electric field is applied, the oppositely charged electrodes induce a Maxwell stress on the elastomer, causing it to stretch laterally and decrease vertically (z-axis) due to Coloumb force [6]. Once the electric field is removed, they return to their original shape. In simpler terms, they can be thought of as compliant capacitors. DEAs have been shown to achieve actuation strains greater than 100% [7]. These positive results are due to prestretching the elastomer by a computed amount and then mounting it onto a rigid frame [8]. Additionally, pre-stretching the elastomeric membrane has been found to increase the dielectric breakdown strength of the actuator [9]. However, amalgamating prestretched membranes in soft robotic applications poses a challenge due to intractable deformations that are tougher to control [10].

Elastomeric Hydraulically Amplified Self-Healing Electrostatic (e-HASEL) is a form of electrohydraulic actuator that has a similar mechanical structure to DEAs; the only difference is a liquid dielectric injected within the elastomeric housing in a pouch [11]. Moreover, as DEAs are rendered inoperable after dielectric breakdown, the dielectric fluid within the e-HASEL was proven to "self-heal" by sealing in the affected areas. Owing to a lower Youngs modulus of the liquid dielectric, e-HASELs can yield larger strains than DEAs. In a similar vein to DEAs, e-HASELs are compliant capacitors and provide the ability for self-sensing and, thereby, providing the ability for closed-loop control by measuring the capacitance between the electrodes [12].

Electro-ribbon actuators (ERA) are are the latest state-of-the-art electrostatic devices that clamp down upon activation [13]. Their mechanical design is much simpler than that of DEAs and elastomeric HASELs, consisting of a high-permittivity insulating layer (such as electrical insulation tape), a conducting layer (thin metal strips), and a liquid dielectric (silicone oil) applied as a bead at the zipping foci. In contrast to DEAs and elastomeric HASELs, ERAs operate on the principle of dielectrophoretic liquid zipping (DLZ) [14]. They require significantly less liquid dielectric and no enclosure. The actuators work by oppositely charging the conductors, with the foci being the strongest point of electrostatic force. By adding a small amount of liquid dielectric at the hinges, the forces are amplified and result in visible movement, with the liquid dielectric being kept in place due to dielectrophoretic forces. This retention of liquid dielectric while amplifying electrostatic actuation is known as DLZ [13], and allows the actuator to achieve strains of 99.84% [13]. Additionally, the novel self-locking behavior of these actuators provides an alternative to solenoids and valves [15]. However, a drawback is that due to the lack of housing, repeated actuation can cause the liquid dielectric to leak into the surroundings. Moreover,

their actuation speed is comparatively slower than other electrostatic actuators.

Chapter 3

Design and Fabrication

3.1 Considerations

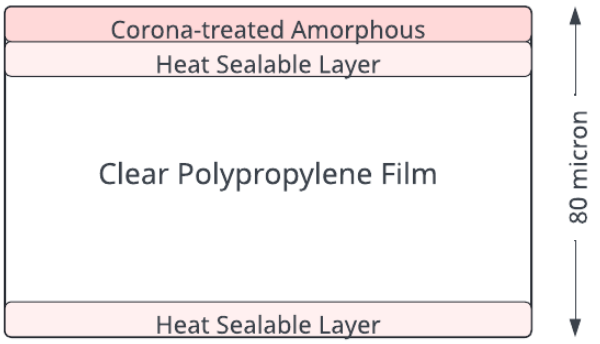

Figure 3.1: Cross-section of L0WS film. The corona-treated layer increases wettability allowing better adhesion of carbon paint.

To build our proposed electrohydraulic actuators, we need to sandwich two layers of thin film that encapsulates a dielectric liquid in a pouch, which is covered with electrodes to provide electrostatic force. We will build the actuators in a rectangular shape for initial development and characterization and finally turn them into a toroidal shape to be used for electrohydraulic haptic muscles in Chapter 7.

Figure 3.2: Charge accumulation at the boundary of the film and electrode visible on the top right corner of the electrode layer (gray).

For electrohydraulic actuators, the type of film used in constructing the pouches is critical in determining the performance of the actuator. The films must have a high dielectric strength to withstand the high voltage needed for actuation. Additionally, to increase wettability and promote adhesion of the electrode material (e.g. carbon paint), the films need to be etched on one side while being heat sealable on the other. Some options for films are biaxially oriented polypropylene (BOPP), polyethylene terephthalate (PET), and thermoplastic polyurethane (TPU). Three different BOPP films were used to build the actuators; however, only the L0WS film (Figure 3.1) proved successful. The other films did not work because when an external electric field is applied, the charge distribution is different across each dielectric layer due to the different dielectric constants. The mismatch leads to an accumulation of charge at the boundary of the two materials, creating sparks, as seen in Figure 3.2. This

effect is known as the Maxwell-Wagner effect [16] [17] [18].

Film	**Thickness** (µm)	**Melting Point** (°C)	**Dielectric Strength** (kV/mm)	**Dielectric Constant**
Fluoropolymer-FEP	50	260 - 280	260	2
Fluoropolymer-PFA	25	300 - 310	260	2
L0WS	20	115 - 190	-	3.5

Table 3.1: List and material properties of the films tested for the fabrication of pouches.

3.2 Fabrication Process

The first step to creating the actuator is to heat seal the film in a defined geometry. Kellaris et al. [19] fabricated a brass die to heat seal the pouches to form a rectangle. A heat press bonded the pouches. While the procedure is straightforward, complex pouch geometries require more effort due to the added challenge of creating new dyes. Furthermore, Mitchell et al. [20] repurposed a 3D printer to heat seal the pouches. They sanded down the printer's nozzle to create a flat surface, preventing it from tearing the film. A silicone layer was placed on the heat-bed to distribute the load evenly. The pouch pattern was then converted to GCODE using the dxf2gcode package on Inkscape. Thick dielectric fluid lubricated the nozzle and the film to reduce friction. While this procedure is easy to replicate and creates complex geometries more quickly than the prior method, problems are still associated with it. For instance, one must perfectly adjust the force between the nozzle and film to achieve a tight seal. The nozzle has to be sanded, thereby altering the 3D printer.

To build upon the above works and improve the process, we carried out two methods of heat sealing: 1) using an impulse sealer 3.4 and 2) deposition of PLA on the films using a commercial 3D printer3.5.

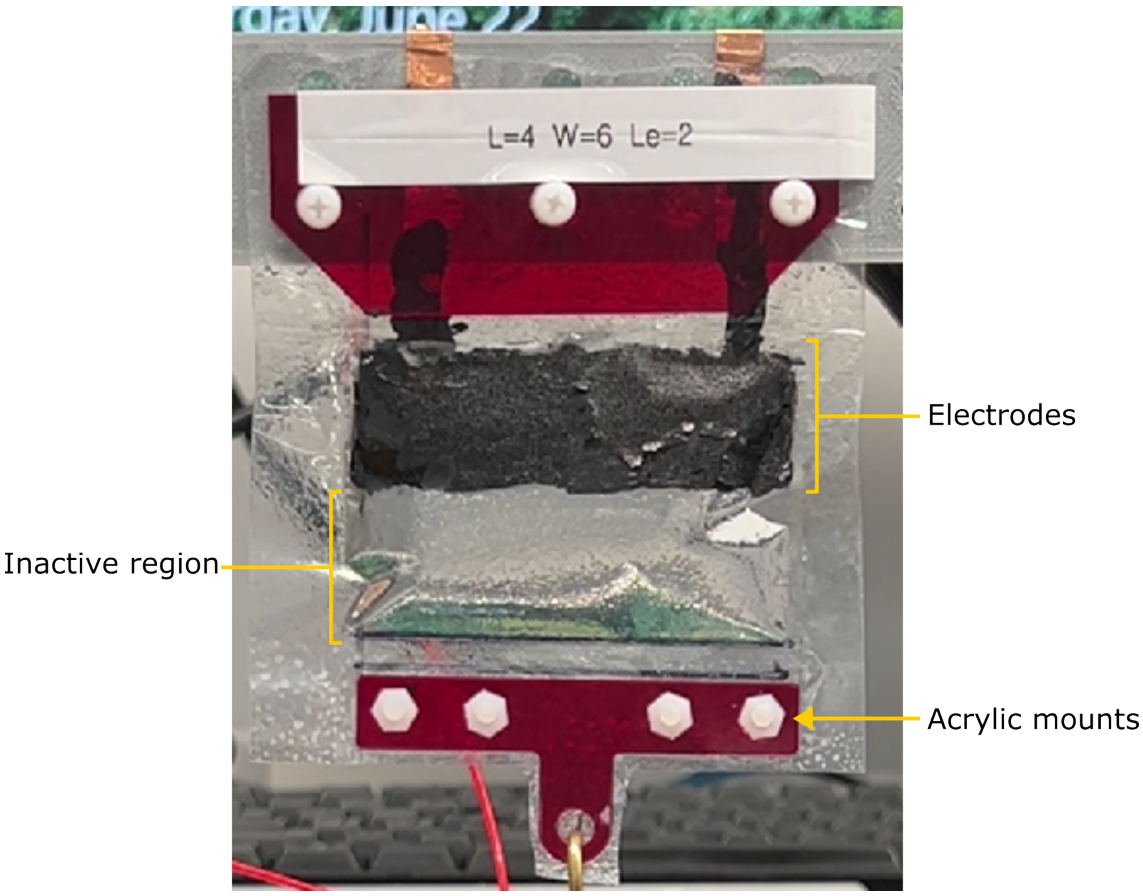

Figure 3.3: Completed actuator

3.2.1 Impulse Sealer

Firstly, an outline of the geometry is hand-drawn on the polypropylene film. An off-the-shelf tabletop impulse sealer bonds the films along the outline. A 3 mm thick heat-resistant silicone sheet is placed below the heating element to provide force dispensing support while heat sealing. A thermally conductive Kapton film is placed above the heating element to protect the film from burning. After performing multiple iterations to calculate the requisite time for heat sealing, it was found to be between 1 and 1.5 seconds.

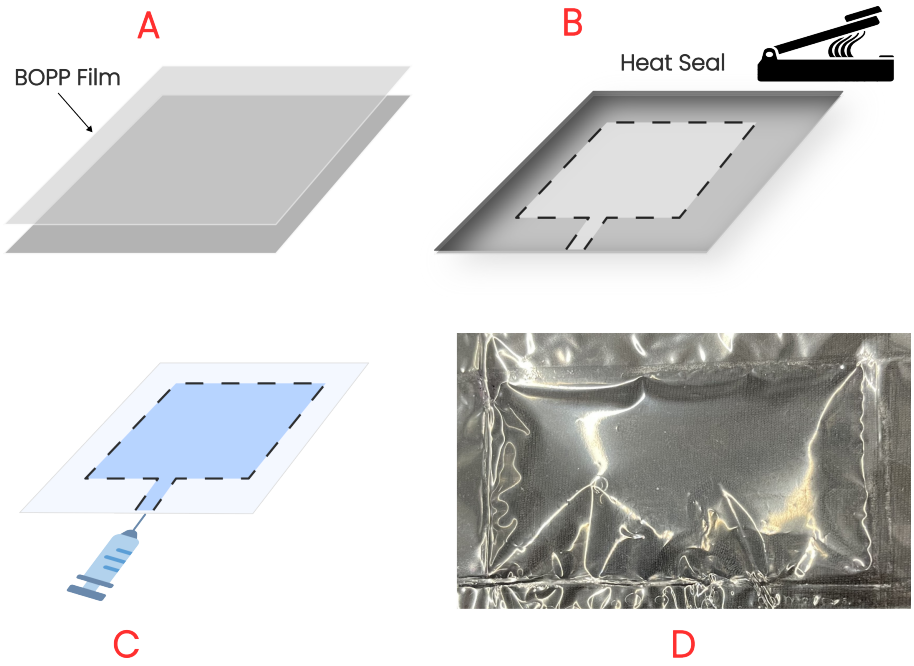

Figure 3.4: Steps for heat sealing use an impulse sealer. (**A**) An outline of the pouch geometry is drawn on one of the films (**B**) Using the table-top impulse sealer, heat along the outline. A double seal is created to prevent any leaks. (**C**) Dielectric liquid is injected into the pouch. (**D**) Final pouch with dielectric fluid.

3.2.2 Deposition of PLA using a 3D-printer

While the impulse sealer method works well to heat pouches quickly, it has some drawbacks. For instance, we can only make rectangular pouches. The inability to create curve outlines is one of the main drawbacks of using the impulse dealing method. As an alternative, we use an off-the-shelf commercial 3-D printer as a heat-sealing tool. Instead of sanding the nozzle or making any additional changes to the 3-D printer, we use it as it is. The first step is to sandwich two films and place them on the heat bed. We use a thermally conductive polyimide film to protect the film and easily distribute the heat. Using a Computer-Aided Design software, we create the geometry of the pouch that is to be sealed, keeping in mind that a fill port is required to fill the liquid. The polypropylene film that is being used melts at 195°C. Therefore, we extrude PLA at 195°C and a print speed of 4 mm/s. The walls of the

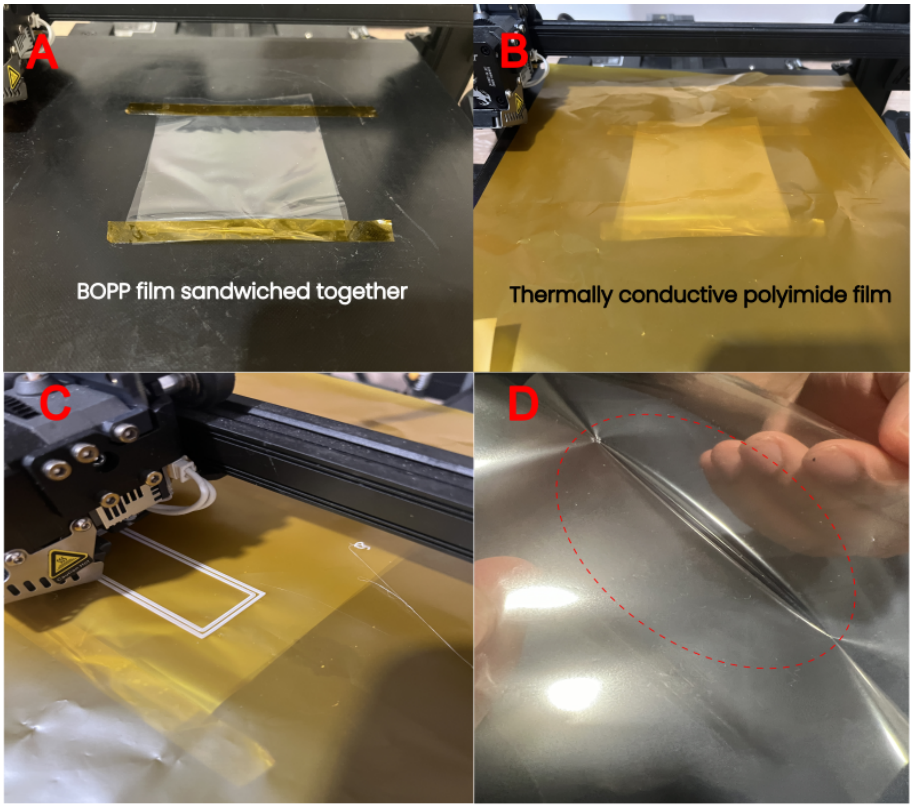

Figure 3.5: Heat sealing pouches using PLA deposition on film

print are 2 mm wide in order to ensure proper seal.

Chapter 4

Mathematical Model

As mentioned in section 3.2, a pouch is manufactured by heat-sealing the BOPP films, injecting the dielectric fluid of the requisite volume into the pouch, and finally, painting the carbon electrodes. The electrodes gradually zip together as an increasing voltage is applied, creating a stroke Δx. In this chapter, we will first derive the volume of the liquid dielectric to be inserted into a pouch with the given dimensions, followed by the determination of output force based on global energy minimization [21].

4.1 Determination of volume of liquid dielectric

Two rectangular films of length L_p, width W, and thickness t are thermally bonded to create the actuator shell. Since the film is flexible and not stretchable, we can assume that there is no elastic energy [22]. Hence, based on these assumptions, the pouches take on a cylindrical shape on full actuation. Let 2α be the central angle, r be the radius of curvature, L_e be the length of the electrodes, and L_p be the arc

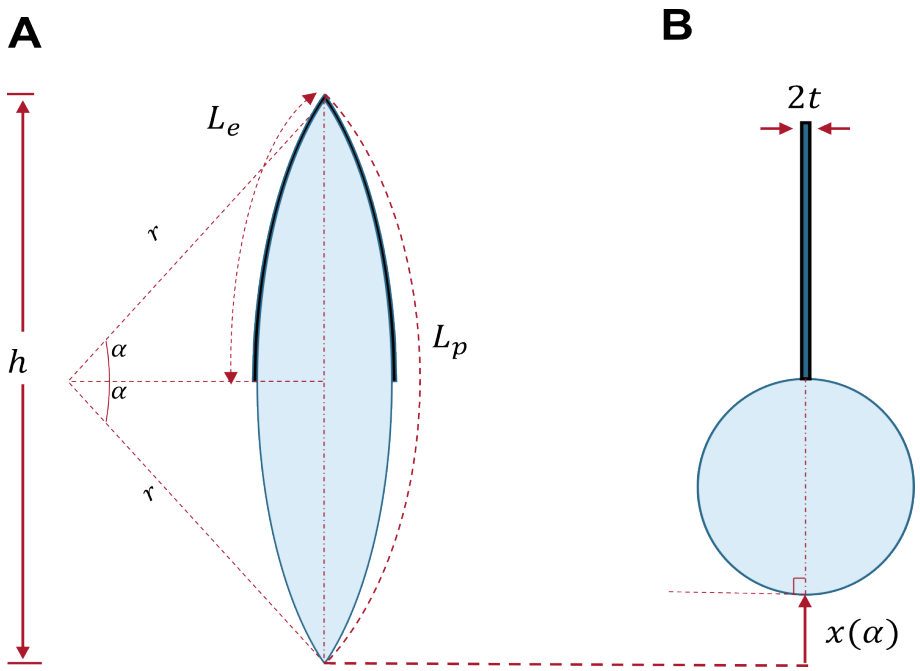

Figure 4.1: Calculation of dielectric volume. (**A**) Actuator at rest (no voltage applied), (**B**) Active region(area uncovered by electrode) attains a circular cross-section

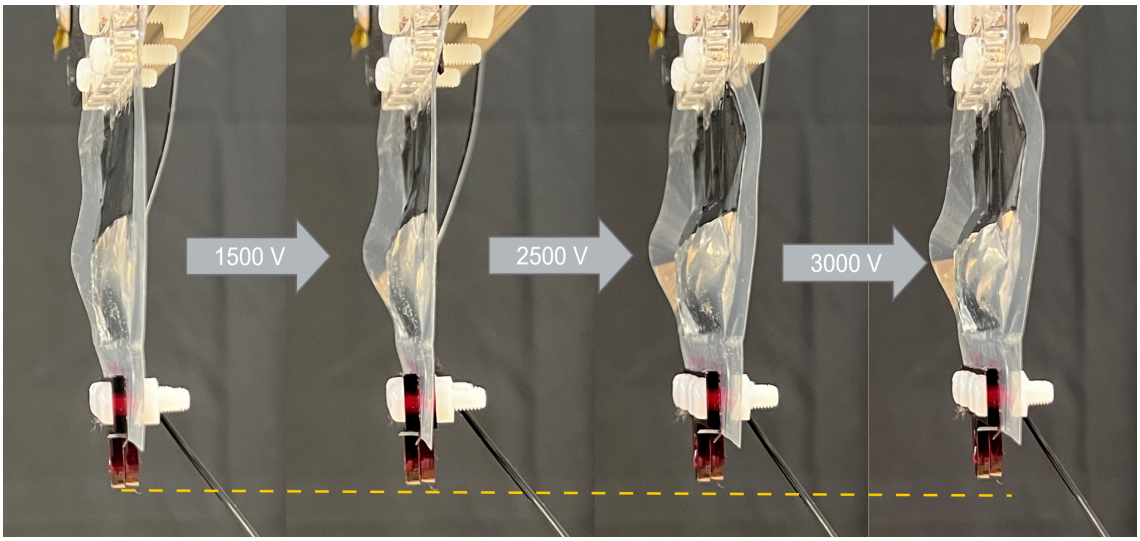

Figure 4.2: Demonstration of zipping actuation. As voltage increases pouch contracts thereby creating stroke Δx

length when the pouch is un-deformed. From geometry, we can show that

$$L_p = 2r\alpha, \tag{4.1}$$

$$rsin\alpha = \frac{h}{2}. \tag{4.2}$$

Solving for h, we obtain the initial length of the actuator as a function of α:

$$h(\alpha) = L_p \frac{sin(\alpha)}{\alpha} \tag{4.3}$$

The volume (Vol) is given by the product of cross-sectional area (A) and width (W):

$$Vol(\alpha) = A \cdot W = \frac{L_p^2 W}{2}(\frac{\alpha - sin(\alpha)cos(\alpha)}{\alpha^2}). \tag{4.4}$$

The stroke (x) of the actuator is given by:

$$x = \sqrt{\pi A}\left(1 - \frac{2}{\pi}\right) - \sqrt{\frac{A}{\alpha - \sin\alpha}}\left(\alpha - 2\sin\frac{\alpha}{2}\right). \tag{4.5}$$

4.2 Determination of Force

The global energy balance equation comprises of the voltage applied to the actuator, an external force acting on the actuator, and electrostatic potential energy within the actuator. The total free energy of the system is given by

$$U_e = E_m + E_e \tag{4.6}$$

Only the zipped region of the electrohydraulic actuators contributes to the electrostatic energy and is given by:

$$U_e = \frac{1}{2}\frac{Q^2}{C(\alpha)} = \frac{1}{2}\frac{(CV)^2}{C(\alpha)} = \frac{1}{2}CV^2 \tag{4.7}$$

where Q is charge and C is capacitance,

$$C(\alpha) = \frac{\epsilon W}{2t} \cdot L_e(\alpha)$$

Work done by a constant force is give by,

$$E_m = Fx(\alpha) \tag{4.8}$$

The electrical energy contributed by the voltage source when supplying charges Q to the pouches and is given by:

$$E_e = QV = CV^2 \tag{4.9}$$

Putting eqs. 4.2, 4.8, 4.9 into 4.7, we can calculate:

$$\frac{1}{2}CV^2 = Fx(\alpha) + CV^2,$$

and hence the external force as:

$$F = -\frac{V^2}{2}\frac{C(\alpha)}{x(\alpha)} \tag{4.10}$$

Chapter 5

High-Voltage Power Supply

5.1 Introduction

High voltage is often necessary for electrostatic actuation in soft robotic applications, but current power supply solutions are bulky and are wall-mounted, limiting mobility. Portable power supplies, on the other hand, can deliver the required high voltages in a compact form, opening up a world of possibilities for deploying soft robots in various environments, from wearable devices to field-based applications. This portability is not just essential; it's the future of fully realizing the potential of soft robotics in healthcare, exploration, and other areas that require lightweight, flexible, and mobile robotic systems.

Lenz et al. [23]present a compact and cost-effective solution for generating high voltages required by Dielectric Elastomer Actuators (DEA). Using a resonant converter with a Greinacher voltage doubler, the researchers have minimized complexity and power consumption, making the technology more accessible at less than €10. Their design achieves low power consumption, under 1.5 W, while reliably driving DEAs and demonstrating consistent performance. However, the system does have

limitations, particularly its sensitivity to load changes, which result in significant drops in output voltage as load resistance increases. Additionally, using a simple passive discharging stage further reduces the voltage. The absence of active control and discharging features limits the design's flexibility for more demanding applications.

Developing battery-operated high-voltage power supplies that can independently control multiple soft robots is crucial for advancing the versatility and autonomy of complex systems. Drawing inspiration from micro-electromechanical systems (MEMS), reducing the operating voltage of electrostatic actuators can lead to simpler circuits, smaller components, and lower costs. Lower voltage systems are more accessible, easier to insulate, and can integrate with existing miniature electronics, ultimately reducing the overall complexity of the driving electronics and making the systems more compact and affordable. However, reducing voltage while maintaining the same power output requires increasing current, which brings forth new challenges. Higher currents elevate safety risks, particularly the potential for harmful electrical discharges that can lead to serious health hazards such as ventricular fibrillation [24]. Thus, while lowering voltage simplifies the system, it simultaneously increases current-related safety concerns, complicating the overall design.

Table 5.1: Comparison of high-voltage power supplies used for electrostatic actuation.

Name	Voltage rating	Weight	Cost
TREK 50/12 [25]	±50kV	136kg	30,000 $
Stanford Research Systems [26]	20kV	4kg	10,000 $
This thesis	5kV	200g	300 $

5.2 Operating Principle and Circuit Design

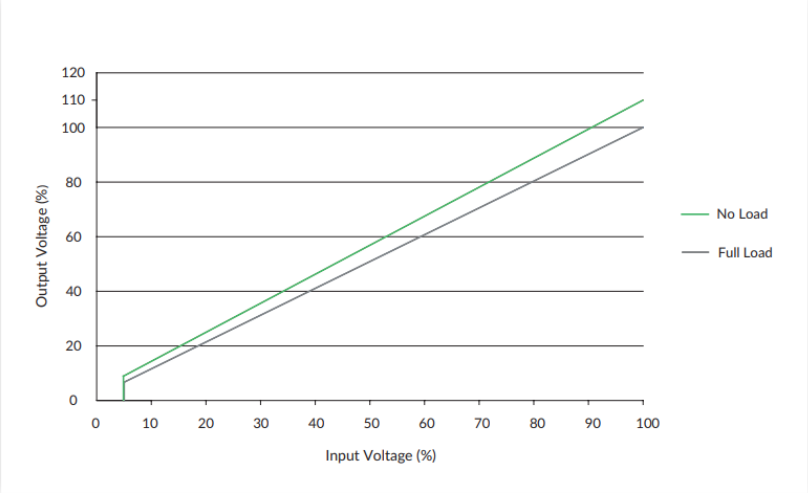

Figure 5.1: Input vs. Output voltage relation of XP-Power G50

The high-voltage amplifier selected for this application is the XP-Power G50, chosen for its galvanic isolation, low electromagnetic interference, and small PCB footprint. However, due to its compact size, external control circuitry is necessary. In the absence of a load, the G50's high-voltage output shows a relatively linear response after an input voltage of 0.7V, but becomes non-linear, as seen in figure 5.1, when a load is connected, necessitating voltage regulation. To address this, an STM32 microcontroller is used to generate a PWM signal to control a buck converter5.2, which in turn regulates the high-voltage amplifier.

The high-voltage amplifier selected for this application is the XP-Power G50, chosen for its galvanic isolation, low electromagnetic interference, and small PCB footprint. However, due to its compact size, external control circuitry is necessary. In the absence of a load, the G50's high-voltage output shows a relatively linear response after an input voltage of 0.7V, but becomes non-linear when a load is connected, necessitating voltage regulation. To address this, an STM32 micro-

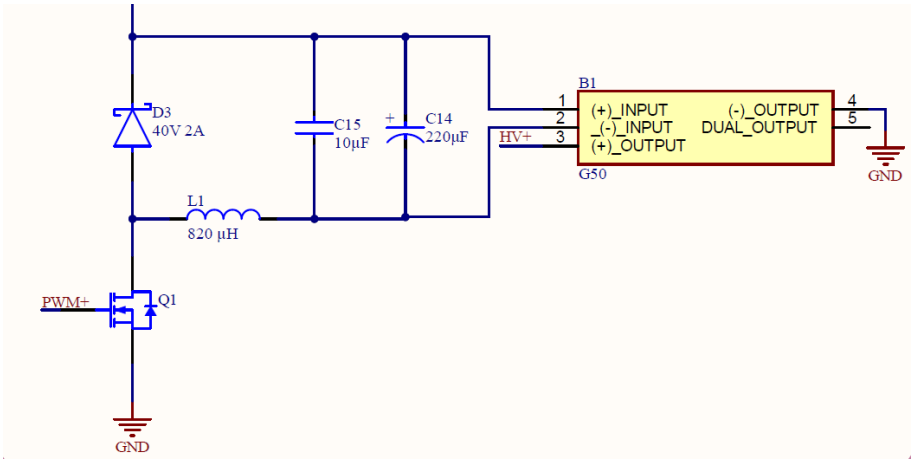

Figure 5.2: Buck converter used to control the G50 amplifier.

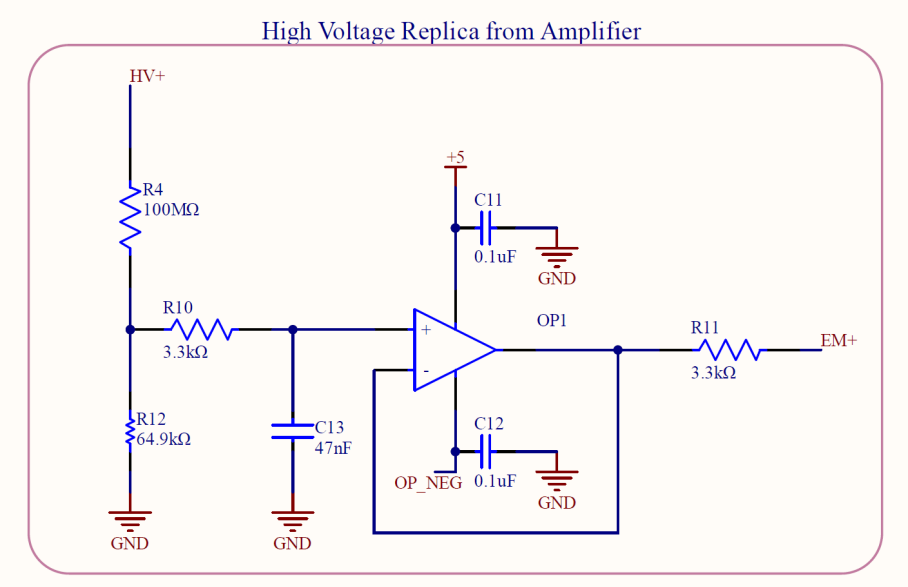

Figure 5.3: Voltage monitoring circuit

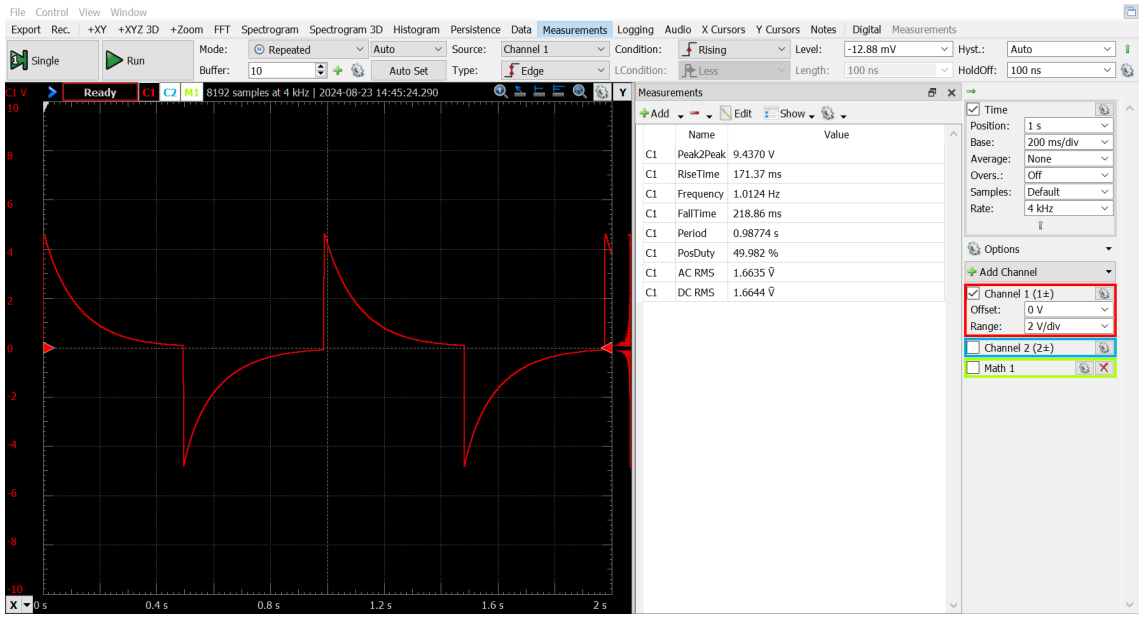

Figure 5.4: Switching output at 5kV

controller is used to generate a PWM signal to control a buck converter, which in turn regulates the high-voltage amplifier. Using the application report from Texas Instruments [27] as the building block for the design of buck converter.

To monitor the output voltage, a replica of the high-voltage is created using a large resistor divider network created from resistors R4 and R12. To minimize the current draw the replica voltage is buffered using an op-amp (OP1) in a voltage follower configuration [28]. Axial thick-film 1% resistors are used to provide approximately 1% accuracy. The output voltage, EM+, is fed to a 12-bit ADC input of the microcontroller. The PID controller regulates the high-voltage by controlling the PWM signal sent to buck converter. A square wave output is generated using a high-voltage optocoupler (OPTO-150). The optocouplers are designed as 100 μA current sources with a Photodiode reverse voltage of 15 kV. A square wave from the microcontroller controls transistors OC1 and OC2, allowing current to flow to the optocoupler LEDs. When the output is OFF, the capacitive load safely discharges to ground through a 250 MΩ bleeder resistor.

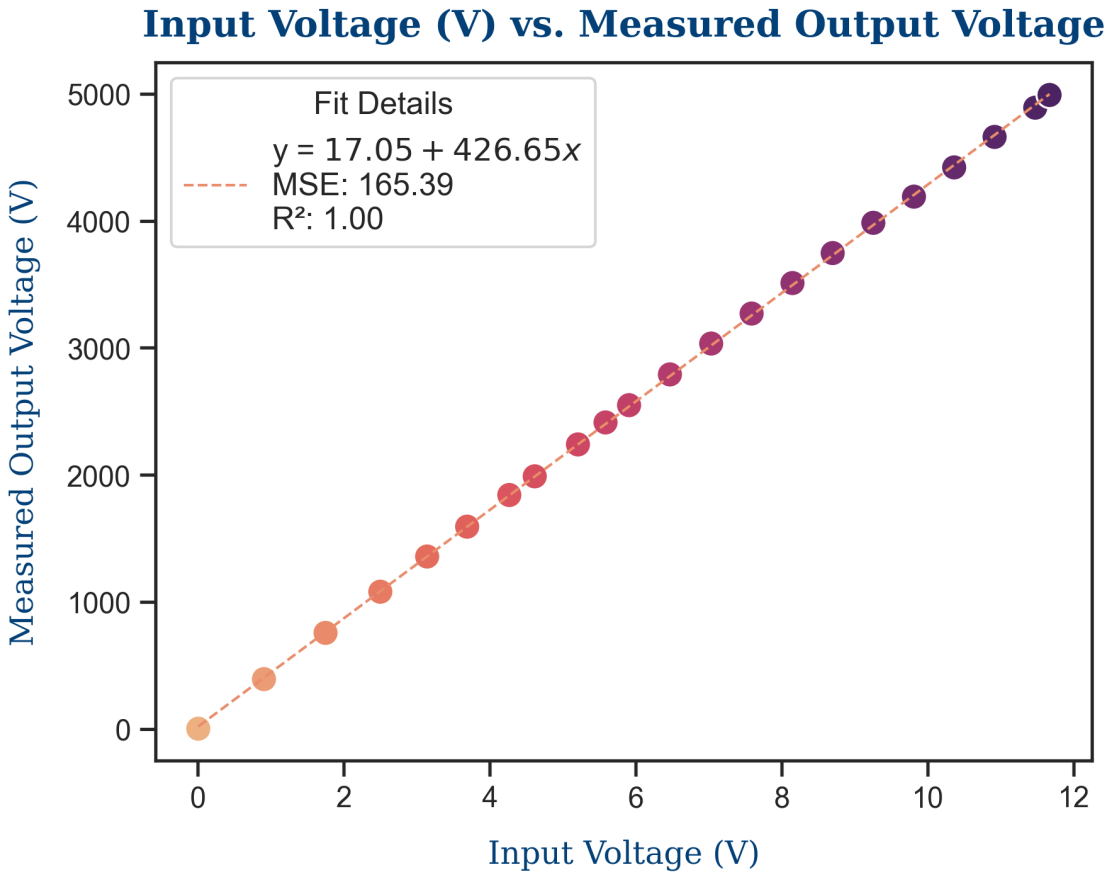

Figure 5.5: Calibration of power supply

Chapter 6

Experiments

6.1 Experimental Setup

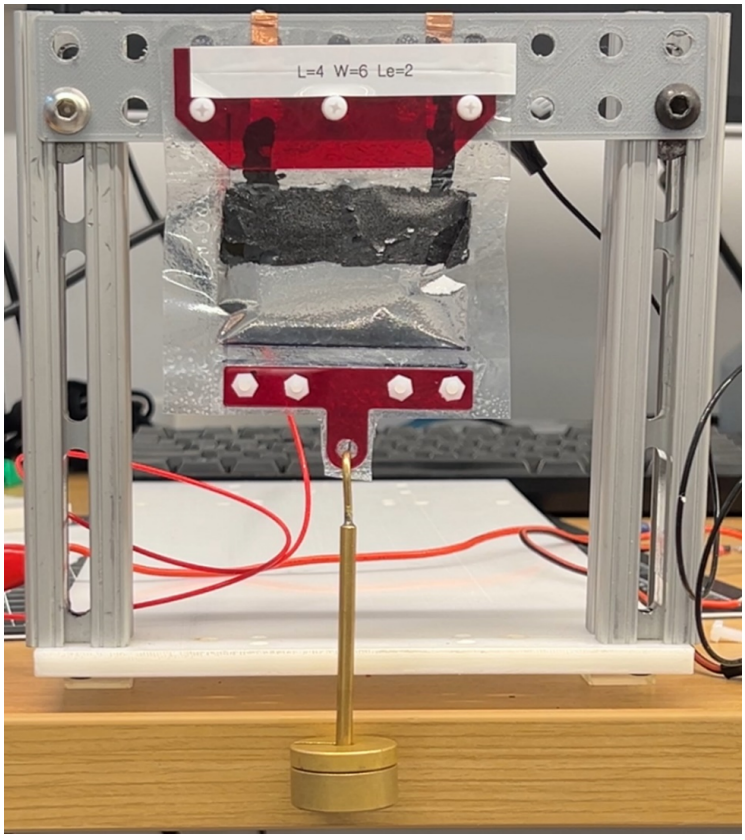

Figure 6.1: Test setup to measure static and dynamic characteristics of the actuator

The experimental setup illustrated in figure 6.1 consists of the electrohydraulic actuator mounted within an aluminum rigid frame. Acrylic mounts (in red) are attached to the actuator with nylon screws along with copper tape at the top to supply the actuator with an external power supply. Brass weight is suspended from the bottom of the actuator, serving as a load to measure the displacement and force output of the actuator when it is activated. The pouches measure 4 cm in length and 6 cm in width and have a liquid dielectric volume of 8 mL. The length of the electrode is 2 cm in length and 5.8 cm in width.

6.2 Static Characteristics

6.2.1 Displacement

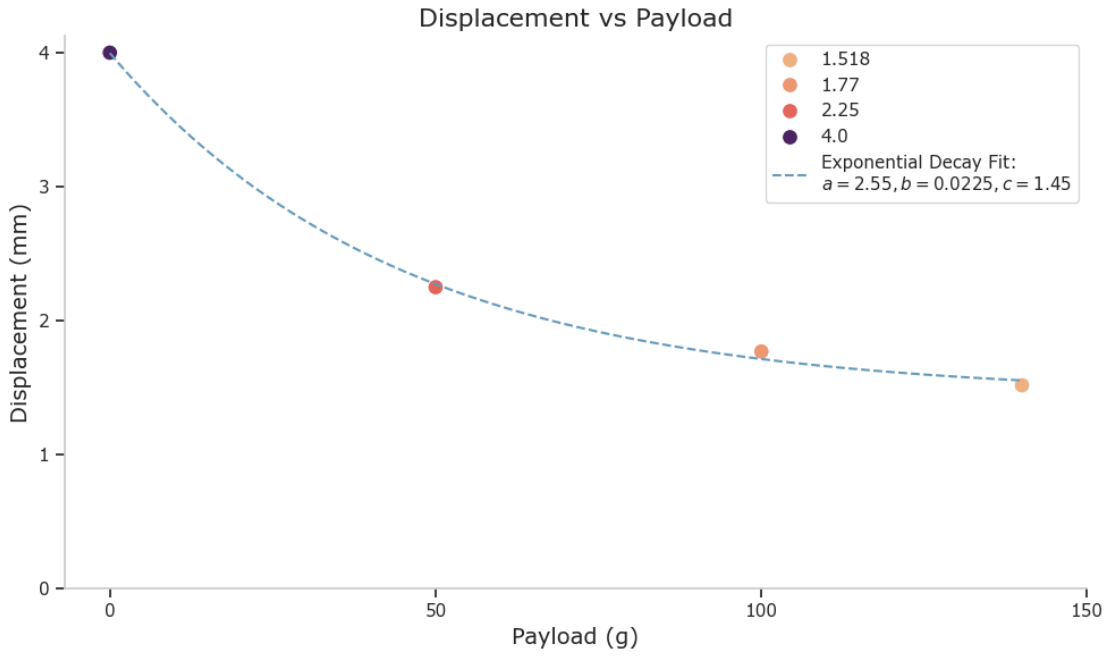

Figure 6.2: Displacement(mm) vs. Payload(g) with an exponential decay fit

The results depicted in figure 6.2 demonstrate that the stroke of the electrohy-

draulic actuator decreases exponentially as the applied payload increases. Initially, with lower payloads, the actuator exhibits a more significant stroke, evident from the maximum displacement of around 4 mm at the 0 gram. As the payload increases, the displacement reduces, demonstrating a diminishing ability of the actuator to contract. This relationship follows an exponential decay pattern, as described by the fitted curve, where parameters a=2.55, b=0.0225, and c=1.45 define the decay rate and shape of the curve. These results suggest that the actuator's performance in terms of displacement is more sensitive to smaller loads, with a more gradual reduction in displacement as the payload increases beyond the free stroke value. Increasing the dimension of the active region would display larger stroke.

6.2.2 Force

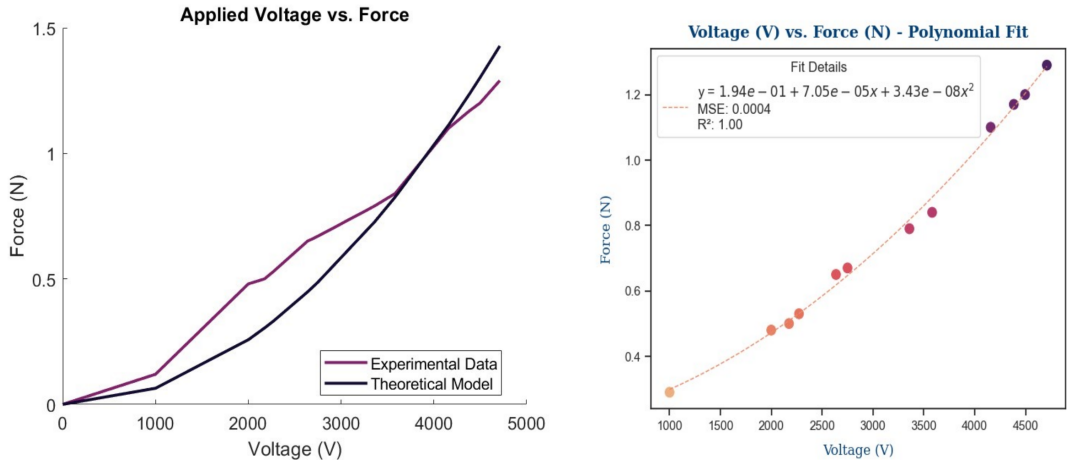

Figure 6.3: (**Left**)Comparison of experimental and theoretical model for Force (**Right**) Polynomial fit of Voltage vs. Force

The left figure compares the experimental data to the theoretical model. The plots display a nonlinear increase in force as voltage rises, which is consistent with the quadratic dependence of force on the electric field. While the experimental data typically follows the theoretical value, small deviations at lower voltages may arise

from material imperfections or sensor noise. Additionally, the polynomial fit on the right has a notably small higher-order term, indicating a linear relationship between force and voltage with small non-linearities. These results support the claim that output force follows a quadratic relationship with respect to voltage, and the fluid pressure within the pouch, also called Maxwell's pressure, is the mechanism driving the actuator's force response across the applied voltage range.

6.3 Transient Response

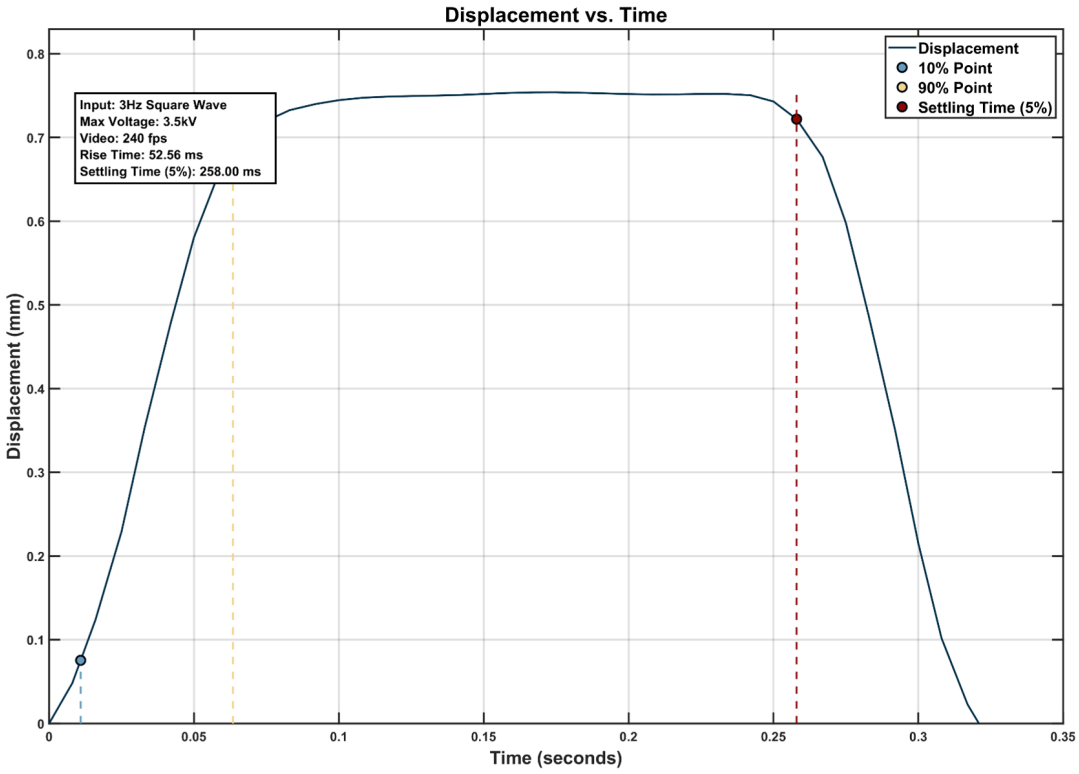

Figure 6.4: Transient response characteristic of the actuator given a 3.5 kV step input

We carried out a transient response analysis to compare the electrohydraulic actuator's dynamic characteristics with those of a pneumatic haptic muscle. We

used a 3.5kV square wave with a frequency of 3Hz as the actuator's input. The actuation was then recorded at 240 frames per second and analyzed using Physlet Tracker software [29].

The transient response gives us a better understanding of the actuator's dynamics under a step input. The quick initial rise in displacement indicates that the actuator responds rapidly to the input, moving towards its maximum stroke length with celerity. The actuator transitions into a steady state, and since there are little to no oscillations, the system is critically damped. The final flat section of the curve indicates that the actuator stabilizes and maintains its position, highlighting its capability for precise and controlled actuation. The plot suggests that the actuator demonstrates a fast and stable response, making it suitable for applications requiring prompt movement and reliable steady-state performance.

Type of Actuator	**Linear Strain** %	**Specific Energy** J/kg
Mammalian muscle [30]	20	40
DEA [31]	3-30	<20
Elastomeric HASEL [11]	124	70
Electro-ribbon [13]	99.84	6.88
This thesis	10	6.76

Table 6.1: Comparison of actuator parameters

Chapter 7

Application: Haptic Muscles

7.1 Overview

Haptics refers to the sense of touch. The science of haptics is divided into kinesthetic and tactile perception. Kinesthetic perception deals with the motion of body parts in relation to each other and the forces exerted by body muscles [32] [33]. In comparison, tactile perception relies on receptors on the skin to feel texture and pressure sensations. Some examples of haptics we see around us are vibration-based haptics, where tiny motors placed in gaming controllers vibrate to provide a sensory substitution instead of a real force. In this work, we target the application of restoring forces on the finger joints of a user as a form of kinesthetic haptic feedback as our research group has done with pneumatic actuators in the past [34], [35], [36], [37].

The operation of the haptic muscles addressed in this thesis is similar to mechanical impedance. As depicted in Figure 7.1, we engineer the muscles to take on a toroidal shape when activated. The active section of the electrohydraulic actuators deforms into a toroid, generating resistance around the user's knuckles. This resistance creates the sensation of gripping an object. Additionally, we investigate

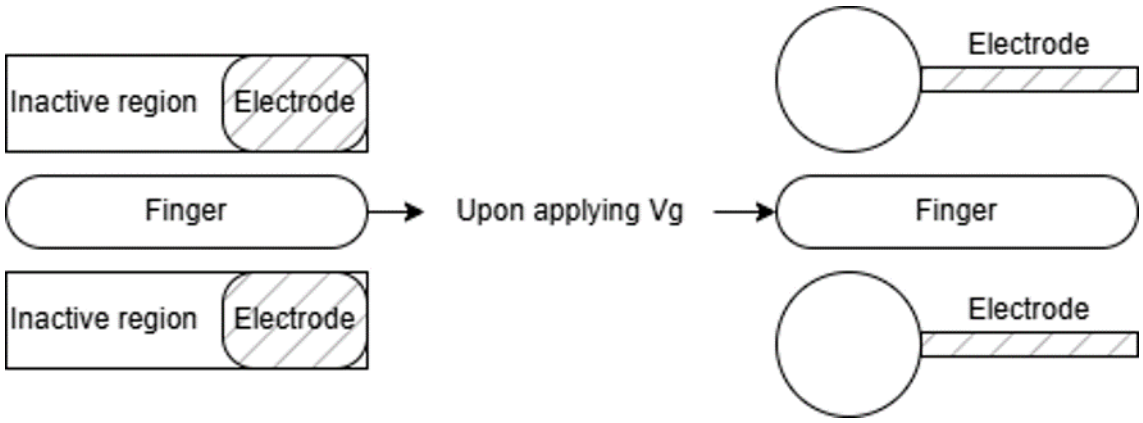

Figure 7.1: Torroidal geometry of haptic muscle

the relationship between force and input voltage.

7.2 Test setup

To create the haptic muscles, we modified rectangular actuators into cylinders by rolling them and heat-sealing the edges to form a snug fit around the finger. The diameter of the finger, which is 6 cm, determined the width of the rectangular pouch. As a safety measure due to the high voltages involved, we utilized a cable-driven 3D-printed artificial finger made of Thermoplastic Polyurethane (TPU). This artificial finger was affixed to a 3D-printed base, and a cable was pulled to flex the finger. It was then connected to a load cell to measure the restoration force.

In this test setup, the finger is initially flexed as seen in Figure 7.2 and the electrohyrdaulic haptic muscle is wrapped around the knuckle in a toroidal shape flexed with the finger as shown in Figure 7.3. When actuated, the muscle tries to go back to a straight toroidal shape, which causes a restoration force, trying to extend the finger.

Figure 7.2: Side view of test setup for haptic muscle

Figure 7.3: Haptic muscle upon application of voltage

7.3 Results

As the voltage increases from 0V to 3500V, the restoration force rises almost linearly. The generated force is minimal at voltages below 1000V, indicating that the muscle requires a specific threshold voltage to initiate significant deformation. However, as the voltage increases beyond 2000V, the restoration force increases rapidly, reaching a peak of around 0.175 N at 3500V. This trend shows that higher voltages enable the actuator to produce stronger restoration forces, meaning its performance can be adjusted by controlling the voltage input.

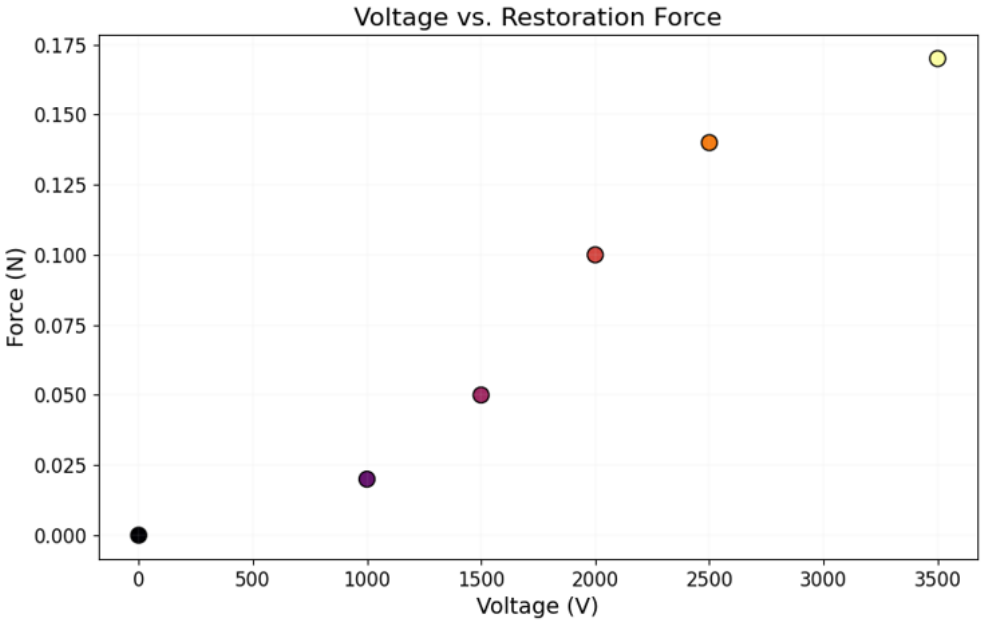

Figure 7.4: Voltage controlled force

Chapter 8

Conclusion

In conclusion, the thesis expounds on a pioneering fabrication technique for producing electrohydraulic actuators. This method presents an economical approach to crafting flexible electrohydraulic transducers. The actuators are powered by high voltages in the kilovolt range, and a smart, portable power supply was engineered using readily available components to ensure efficient and secure operation. Moreover, these actuators were utilized as haptic muscles to gauge restoration forces, showcasing their potential in Virtual Reality (VR) and teleoperation applications. This research marks a significant step forward in soft actuators, offering an accessible method for creating haptic devices boasting kinaesthetic feedback capacities.

Driving forward, we have identified a few areas for further advancement. To enhance user safety, we plan to cover the actuators with a thin layer of silicone to prevent electrical shocks. Additionally, we will explore alternative bonding methods to replace the current heat-sealing process, as it can cause micro-tears in the film, potentially affecting durability. We will also investigate new electrode materials such as hydrogels, electro-active polymers, and other smart materials to improve the performance of the actuators. Furthermore, we aim to use additive manufactur-

ing techniques to print electrodes directly onto the pouches, which will help reduce manufacturing time and complexity. Lastly, we plan to build circuitry to measure capacitance by leveraging the actuators' self-sensing capabilities, enabling more precise control through closed-loop feedback. These advancements will continue to push the boundaries of soft transducer technology and worldwide adoption.

Bibliography

[1] Daniela Rus and Michael T. Tolley. Design, fabrication and control of soft robots. *Nature*, 521(7553):467–475, May 2015.

[2] Gursel Alici. Softer is harder: What differentiates soft robotics from hard robotics? *MRS Advances*, 3:1–12, 02 2018.

[3] Yufei Hao, Shixin Zhang, Bin Fang, Fuchun Sun, Huaping Liu, and Haiyuan Li. A review of smart materials for the boost of soft actuators, soft sensors, and robotics applications. *Chinese Journal of Mechanical Engineering*, 35(1):37, Apr 2022.

[4] Feng Du, Shu Wang, Zhihao Chen, and Quan Li. Stimuli responsive actuators: recent advances. *J. Mater. Chem. C*, 12:8217–8242, 2024.

[5] Federico Carpi, Danilo De Rossi, Roy Kornbluh, Ronald Edward Pelrine, and Peter Sommer-Larsen. *Dielectric elastomers as electromechanical transducers: Fundamentals, materials, devices, models and applications of an emerging electroactive polymer technology.* Elsevier, 2011.

[6] Zhigang Suo. Theory of dielectric elastomers. *Acta Mechanica Solida Sinica*, 23(6):549–578, 2010.

[7] R Pelrine, R Kornbluh, Q Pei, and J Joseph. High-speed electrically actuated elastomers with strain greater than 100%. *Science*, 287(5454):836–839, February 2000.

[8] Guggi Kofod. The static actuation of dielectric elastomer actuators: how does pre-stretch improve actuation? *Journal of Physics D: Applied Physics*, 41(21):215405, oct 2008.

[9] Guo-Ying Gu, Jian Zhu, Li-Min Zhu, and Xiangyang Zhu. A survey on dielectric elastomer actuators for soft robots. *Bioinspiration & biomimetics*, 12(1):011003, 2017.

[10] Samuel Rosset, Oluwaseun A Araromi, Jun Shintake, and Herbert R Shea. Model and design of dielectric elastomer minimum energy structures. *Smart Materials and Structures*, 23(8):085021, jul 2014.

[11] E. Acome, S. K. Mitchell, T. G. Morrissey, M. B. Emmett, C. Benjamin, M. King, M. Radakovitz, and C. Keplinger. Hydraulically amplified self-healing electrostatic actuators with muscle-like performance. *Science*, 359(6371):61–65, 2018.

[12] Cosima Schunk, Levi Pearson, Eric Acome, Timothy G Morrissey, Nikolaus Correll, Christoph Keplinger, Mark E Rentschler, and J Sean Humbert. System identification and closed-loop control of a hydraulically amplified self-healing electrostatic (hasel) actuator. In *2018 IEEE/RSJ International Conference on Intelligent Robots and Systems (IROS)*, pages 6417–6423. IEEE, 2018.

[13] Majid Taghavi, Tim Helps, and Jonathan Rossiter. Electro-ribbon actuators and electro-origami robots. *Science Robotics*, 3(25):eaau9795, 2018.

[14] Herbert A. Pohl. The Motion and Precipitation of Suspensoids in Divergent Electric Fields. *Journal of Applied Physics*, 22(7):869–871, 07 1951.

[15] Majid Taghavi, Tim Helps, and Jonathan Rossiter. Characterisation of self-locking high-contraction electro-ribbon actuators. In *2020 IEEE International Conference on Robotics and Automation (ICRA)*, pages 5856–5861. IEEE, 2020.

[16] Changsheng Li, Gangjin Chen, Xunlin Qiu, Qiwei Lou, and Xiaoli Gao. A direct proof for Maxwell–Wagner effect of heterogeneous interface. *AIP Advances*, 11(6):065227, 06 2021.

[17] Thi Thu Nga Vu, Gilbert Teyssedre, Séverine Le Roy, and Christian Laurent. Maxwell–wagner effect in multi-layered dielectrics: Interfacial charge measurement and modelling. *Technologies*, 5(2), 2017.

[18] Mitsumasa Iwamoto. *Maxwell–Wagner Effect*, pages 1276–1285. Springer Netherlands, Dordrecht, 2012.

[19] Nicholas Kellaris, Vidyacharan Gopaluni Venkata, Garrett M. Smith, Shane K. Mitchell, and Christoph Keplinger. Peano-hasel actuators: Muscle-mimetic, electrohydraulic transducers that linearly contract on activation. *Science Robotics*, 3(14):eaar3276, 2018.

[20] Shane K. Mitchell, Xingrui Wang, Eric Acome, Trent Martin, Khoi Ly, Nicholas Kellaris, Vidyacharan Gopaluni Venkata, and Christoph Keplinger. An easy-to-implement toolkit to create versatile and high-performance hasel actuators for untethered soft robots. *Advanced Science*, 6(14):1900178, 2019.

[21] Giacomo Moretti, Mattia Duranti, Michele Righi, Rocco Vertechy, and Marco Fontana. Analysis of dielectric fluid transducers. In Yoseph Bar-Cohen, editor, *Electroactive Polymer Actuators and Devices (EAPAD) XX*, volume 10594, page 105940W. International Society for Optics and Photonics, SPIE, 2018.

[22] Ryuma Niiyama, Daniela Rus, and Sangbae Kim. Pouch motors: Printable/inflatable soft actuators for robotics. In *2014 IEEE International Conference on Robotics and Automation (ICRA)*, pages 6332–6337, 2014.

[23] S. Lenz, B. Holz, S. Hau, and S. Seelecke. Development of a high voltage source for dielectric elastomer actuators (dea). In *ACTUATOR 2018; 16th International Conference on New Actuators*, pages 1–4, 2018.

[24] S Pourazadi, A Shagerdmootaab, H Chan, M Moallem, and C Menon. On the electrical safety of dielectric elastomer actuators in proximity to the human body. *Smart Materials and Structures*, 26(11):115007, oct 2017.

[25] trek. `https://www.advancedenergy.com/getmedia/06e93b4c-968b-459e-a35b-31a8758886f1/en-hv-amplifier-trek-50-12-data-sheet.pdf`.

[26] stanford. `https://www.advancedenergy.com/getmedia/06e93b4c-968b-459e-a35b-31a8758886f1/en-hv-amplifier-trek-50-12-data-sheet.pdf`.

[27] ti.com. `https://www.ti.com/lit/an/slva477b/slva477b.pdf?ts=1724545570818`.

[28] xppower. `https://www.xppower.com/products/series/resources/HV_Monitors.pdf`.

[29] tracker. `https://physlets.org/tracker/`.

[30] John Madden, Nathan Vandesteeg, Patrick Anquetil, Peter Madden, Arash Takshi, Rachel Pytel, Serge Lafontaine, Paul Wieringa, and Ian Hunter. Artificial muscle technology: Physical principles and naval prospects. *Oceanic Engineering, IEEE Journal of*, 29:706 – 728, 08 2004.

[31] Ronald E. Pelrine, Roy D. Kornbluh, and Jose P. Joseph. Electrostriction of polymer dielectrics with compliant electrodes as a means of actuation. *Sensors and Actuators A: Physical*, 64(1):77–85, 1998. Tenth IEEE International Workshop on Micro Electro Mechanical Systems.

[32] Lynette Jones. *Haptics*. The MIT Press, 2018.

[33] Janet L. Taylor. *Kinesthetic Inputs*, pages 931–964. Springer New York, New York, NY, 2013.

[34] Sihui Li, Raagini Rameshwar, Ann Marie Votta, and Cagdas D Onal. Intuitive control of a robotic arm and hand system with pneumatic haptic feedback. *IEEE Robotics and Automation Letters*, 4(4):4424–4430, 2019.

[35] Saraj Pirasmepulkul, Alexander Caracappa, Peerapat Luxsuwong, Cagdas D Onal, William Michalson, Tri Khuu, and Ming Luo. Haptic glove as a wearable force feedback user interface, February 4 2020. US Patent 10,551,923.

[36] Raagini Rameshwar, Erik Howard Skorina, and Cagdas D Onal. Fabric-silicone composite haptic muscles for sensitive wearable force feedback. In *Proceedings of the 16th International Conference on PErvasive Technologies Related to Assistive Environments*, pages 33–41, 2023.

[37] Raagini Rameshwar. *Intuitive Teleoperation of a Robotic Arm and Gripper with Soft Pneumatic Haptic Feedback*. PhD thesis, Worcester Polytechnic Institute, 2023.

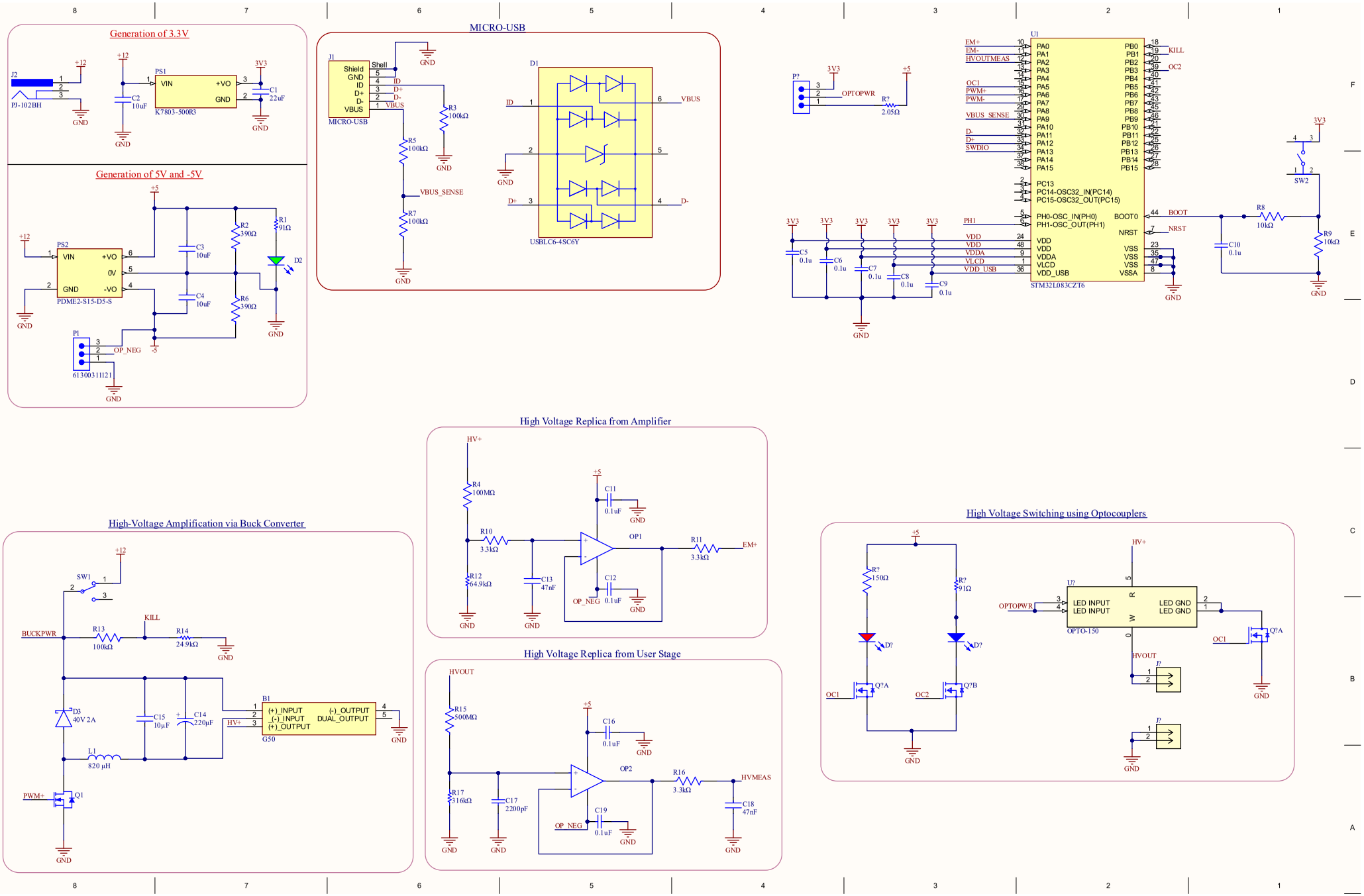
Generation of 3.3V
J2
PJ-102BH
+12
PS1
VIN
+VO
GND
K7803-500R3
3V3
C2
10uF
C1
22uF
Generation of 5V and -5V
+5
+12
PS2
VIN
+VO
0V
GND
-VO
PDME2-S15-D5-S
C3
10uF
C4
10uF
R2
390Ω
R6
390Ω
R1
91Ω
D2
P1
OP_NEG
-5
61300311121
MICRO-USB
J1
Shield
GND
ID
D+
D-
VBUS
MICRO-USB
R3
100kΩ
R5
100kΩ
R7
100kΩ
VBUS_SENSE
D1
USBLC6-4SC6Y
U1
EM+
EM-
HVOUTMEAS
OC1
PWM+
PWM-
VBUS_SENSE
D-
D+
SWDIO
PH1
PA0
PA1
PA2
PA3
PA4
PA5
PA6
PA7
PA8
PA9
PA10
PA11
PA12
PA13
PA14
PA15
PC13
PC14-OSC32_IN(PC14)
PC15-OSC32_OUT(PC15)
PH0-OSC_IN(PH0)
PH1-OSC_OUT(PH1)
VDD
VDD
VDDA
VLCD
VDD_USB
PB0
PB1
PB2
PB3
PB4
PB5
PB6
PB7
PB8
PB9
PB10
PB11
PB12
PB13
PB14
PB15
BOOT0
NRST
VSS
VSS
VSS
VSSA
KILL
OC2
BOOT
NRST
STM32L083CZT6
P?
OPTOPWR
R?
2.05Ω
SW2
R8
10kΩ
R9
10kΩ
C10
0.1u
C5
0.1u
C6
0.1u
C7
0.1u
C8
0.1u
C9
0.1u
High Voltage Replica from Amplifier
HV+
R4
100MΩ
R10
3.3kΩ
R12
64.9kΩ
C13
47nF
OP1
C11
0.1uF
C12
0.1uF
OP_NEG
R11
3.3kΩ
EM+
High Voltage Replica from User Stage
HVOUT
R15
500MΩ
R17
316kΩ
C17
2200pF
OP2
C16
0.1uF
C19
0.1uF
OP_NEG
R16
3.3kΩ
HVMEAS
C18
47nF
High-Voltage Amplification via Buck Converter
SW1
BUCKPWR
R13
100kΩ
KILL
R14
24.9kΩ
D3
40V 2A
C15
10µF
C14
220µF
L1
820 µH
PWM+
Q1
B1
(+)_INPUT
(-)_INPUT
(+)_OUTPUT
(-)_OUTPUT
DUAL_OUTPUT
HV+
G50
High Voltage Switching using Optocouplers
R?
150Ω
R?
91Ω
D?
D?
OC1
Q?A
OC2
Q?B
U?
LED INPUT
LED INPUT
LED GND
LED GND
OPTO-150
OPTOPWR
HVOUT
J?
J?
Q?A
OC1

Oscilloscope plots for calculation of rise time

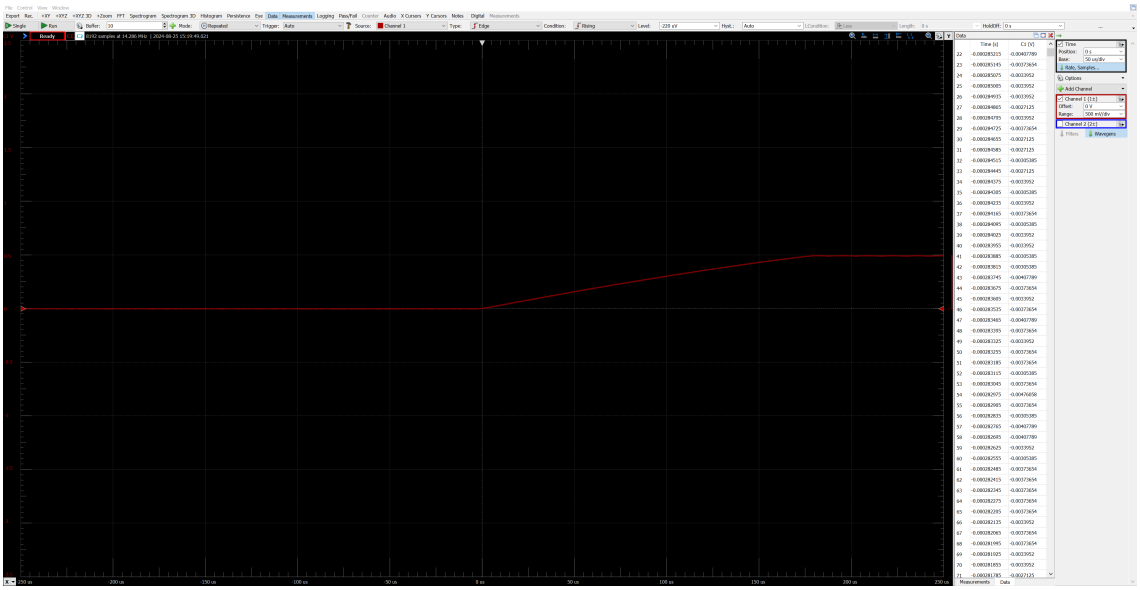

Figure 1: Rise time 500V